

Discrete Boltzmann model for implosion and explosion related compressible flow with spherical symmetry

Aiguo Xu^{a,b,*}, Guangcai Zhang^a, Yudong Zhang^{a,c}, Pei Wang^a, Yangjun Ying^a

^a*National Key Laboratory of Computational Physics, Institute of Applied Physics and Computational Mathematics, P. O. Box 8009-26, Beijing 100088, P.R.China*

^b*Center for Applied Physics and Technology, MOE Key Center for High Energy Density Physics Simulations, College of Engineering, Peking University, Beijing 100871, China*

^c*Key Laboratory of Transient Physics, Nanjing University of Science and Technology, Nanjing 210094, China*

Abstract

To kinetically model implosion and explosion related phenomena, we present a theoretical framework for constructing Discrete Boltzmann Model(DBM) with spherical symmetry in spherical coordinates. To this aim, a key technique is to use *local* Cartesian coordinates to describe the particle velocity in the kinetic model. Thus, the geometric effects, like the divergence and convergence, are described as a “force term”. To better access the nonequilibrium behavior, even though the corresponding hydrodynamic model is one-dimensional, the DBM uses a Discrete Velocity Model(DVM) with 3 dimensions. A new scheme is introduced so that the DBM can use the same DVM no matter considering the extra degree of freedom or not. As an example, a DVM with 26 velocities is formulated to construct the DBM in the Navier-Stokes level. Via the DBM, one can study simultaneously the hydrodynamic and thermodynamic nonequilibrium behaviors in the implosion and explosion process which are not very close to the spherical center. The extension of current model to the multiple-relaxation-time version is straightforward.

Keywords: Discrete Boltzmann Model, compressible flows, spherical symmetry, geometric effects, thermodynamic non-equilibrium

*Corresponding author

Email address: Xu_Aiguo@iapcm.ac.cn (Aiguo Xu)

1. Introduction

Compressible flows are ubiquitous in natural and engineering fields. The study of compressible flow is often associated with the flight of modern high-speed aircraft and atmospheric reentry of space-exploration vehicles; high-Mach-number combustion system [1], hydrodynamic instabilities in inertial confinement fusion [2], materials under strong shock or detonation[3], etc. Common flows which are generally in large scale and slow kinetic mode can be described by the Navier-Stokes equations. It has been known that the Navier-Stokes model encounters problems in describing shock wave, detonation wave, boundary layer, micro flows, and flows with very quick kinetic modes. The physical reasons can be understood as below. According to the Chapman-Enskog analysis, the Navier-Stokes equations are the set of hydrodynamic equations where only the first order Thermodynamic Non-Equilibrium (TNE) in Knudsen number are taken into account. However, the Knudsen numbers in those small structures and quick kinetic modes are not very small, which challenge the validity of Navier-Stokes modeling. At the same time, in the traditional Navier-Stokes modeling the TNE effects are coarsely described by the viscous stress and heat flux with phenomenological constitutive relations.

In recent years, a variety of kinetic models based on Boltzmann equation are proposed to simulate non-equilibrium flows[4–23]. The Discrete Boltzmann Method (DBM) [24–37] recently developed from the Lattice Boltzmann Method (LBM) [38–52] belongs to this category. The Boltzmann equation presents values and evolutions of all kinetic moments of the distribution function. Similar to, but different from, the original Boltzmann equation, the DBM presents not only values and evolutions of conserved kinetic moments (density, momentum and energy) but also those of some nonconserved kinetic moments. The former correspond to those described by hydrodynamic equations, the latter complement the former in finer description of specific status and help to understand the nonlinear constitutive relations of non-equilibrium flows[24, 25]. In recent years, the DBM has brought some new physical insights into the fundamental

mechanisms of various complex flow systems. For example, the TNE intensity has been used to discriminate the spinodal decomposition stage and the domain growth stage in phase separation [28]; the abundant TNE characteristics have been used to distinguish and capture various interfaces [26, 29] in numerical experiments, to investigate the fundamental mechanisms for entropy increase [31] in complex flows. Some of the new observations brought by DBM, for example, the nonequilibrium fine structures of shock waves, have been confirmed and supplemented by the results of molecular dynamics [53–55].

Up to now, most of DBM models for compressible fluids are in Cartesian coordinates, except for the one in polar coordinates [26]. In traditional modeling the implosion and explosion processes, one-dimensional hydrodynamic model is frequently used to describe system with spherical symmetry and system with cylindrical symmetry with translational symmetry. In this work we aim to construct the DBM for compressible flow systems with spherical symmetry.

This paper is organized as below. In section II we briefly review the kinetic and hydrodynamic models of the fluid system. In terms of their correlations, we formulate two set of measures for the deviation of the system from its thermodynamic equilibrium. The discrete Boltzmann models are formulated and some numerical calculation results are shown in section III. Section IV presents the conclusion and discussions.

2. Fluid models

2.1. Kinetic model

The Boltzmann BGK model reads

$$\partial_t f + \mathbf{v} \cdot \nabla f = -\frac{1}{\tau} (f - f^{eq}), \quad (1)$$

where $f = f(\mathbf{R}, \mathbf{v}, t) = f(x, y, z, v_x, v_y, v_z, t)$, $\mathbf{R} = x\hat{\mathbf{x}} + y\hat{\mathbf{y}} + z\hat{\mathbf{z}}$ and $\mathbf{v} = v_x\hat{\mathbf{x}} + v_y\hat{\mathbf{y}} + v_z\hat{\mathbf{z}}$ in Cartesian coordinates.

In spherical coordinates, as shown in Figure 1, the position $\mathbf{R} = r\hat{\mathbf{r}}$. The three parameters r , θ and φ are the radial, azimuth and zenith angle, respectively.

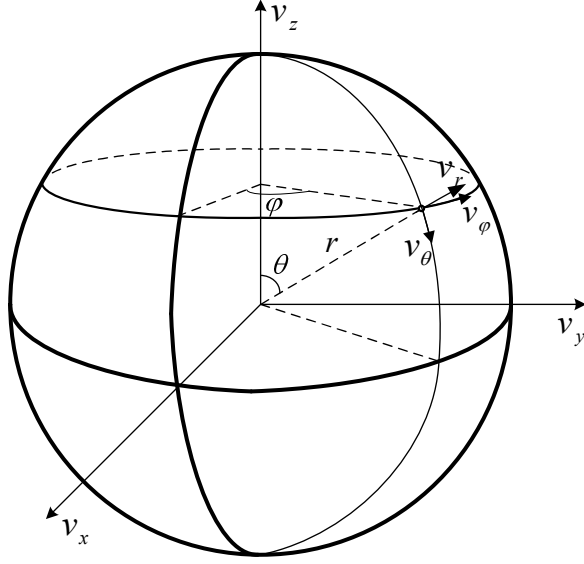


Figure 1: Diagrammatic drawing of spherical coordinate frame and Cartesian coordinate frame.

The unit vectors, $\hat{\mathbf{r}}$, $\hat{\boldsymbol{\theta}}$ and $\hat{\boldsymbol{\varphi}}$, are the changing directions of the position vector \mathbf{R} along the three parameters, r , θ and φ , respectively, i.e.,

$$d\mathbf{R} = \hat{\mathbf{r}}dr + r\hat{\boldsymbol{\theta}}d\theta + r\sin\theta\hat{\boldsymbol{\varphi}}d\varphi.$$

Obviously, $\hat{\mathbf{r}}$, $\hat{\boldsymbol{\theta}}$ and $\hat{\boldsymbol{\varphi}}$ are orthogonal to each other and satisfy the following relationships,

$$\begin{aligned}\hat{\boldsymbol{\varphi}} &= \hat{\mathbf{r}} \times \hat{\boldsymbol{\theta}} \quad , \\ \hat{\boldsymbol{\theta}} &= \hat{\boldsymbol{\varphi}} \times \hat{\mathbf{r}} \quad , \\ \hat{\mathbf{r}} &= \hat{\boldsymbol{\theta}} \times \hat{\boldsymbol{\varphi}} \quad .\end{aligned}$$

It is easy to find that

$$\begin{aligned}d\hat{\mathbf{r}} &= (\hat{\boldsymbol{\varphi}}d\theta + \hat{\mathbf{z}}d\varphi) \times \hat{\mathbf{r}} = \hat{\boldsymbol{\theta}}d\theta + \hat{\boldsymbol{\varphi}}\sin\theta d\varphi, \\ d\hat{\boldsymbol{\theta}} &= (\hat{\boldsymbol{\varphi}}d\theta + \hat{\mathbf{z}}d\varphi) \times \hat{\boldsymbol{\theta}} = -\hat{\mathbf{r}}d\theta + \hat{\boldsymbol{\varphi}}\cos\theta d\varphi, \\ d\hat{\boldsymbol{\varphi}} &= (\hat{\boldsymbol{\varphi}}d\theta + \hat{\mathbf{z}}d\varphi) \times \hat{\boldsymbol{\varphi}} = -(\hat{\mathbf{r}}\sin\theta + \hat{\boldsymbol{\theta}}\cos\theta) d\varphi.\end{aligned}$$

The particle velocity \mathbf{v} can use the any one of the two sets of Cartesian coordinates, $(\hat{\mathbf{x}}, \hat{\mathbf{y}}, \hat{\mathbf{z}})$ and $(\hat{\mathbf{r}}, \hat{\boldsymbol{\theta}}, \hat{\boldsymbol{\varphi}})$, as below:

$$\mathbf{v} = v_x \hat{\mathbf{x}} + v_y \hat{\mathbf{y}} + v_z \hat{\mathbf{z}}$$

or

$$\mathbf{v} = v_r \hat{\mathbf{r}} + v_\theta \hat{\boldsymbol{\theta}} + v_\varphi \hat{\boldsymbol{\varphi}},$$

where $v_r = \mathbf{v} \cdot \hat{\mathbf{r}}$, $v_\theta = \mathbf{v} \cdot \hat{\boldsymbol{\theta}}$ and $v_\varphi = \mathbf{v} \cdot \hat{\boldsymbol{\varphi}}$ are the projections of \mathbf{v} in the $\hat{\mathbf{r}}$, $\hat{\boldsymbol{\theta}}$, and $\hat{\boldsymbol{\varphi}}$ directions, respectively. Correspondingly, the distribution function f can also be described in two different forms,

$$f = f(r, \theta, \varphi, v_x, v_y, v_z, t) \quad (2)$$

or

$$f = f(r, \theta, \varphi, v_r, v_\theta, v_\varphi, t). \quad (3)$$

In this work we will use the latter form, Eq. (3). Under the definition (3), it should be stressed that, when calculate the spatial derivative, ∇f , even though the particle velocity \mathbf{v} is fixed, its three components vary with the position \mathbf{R} , i.e., $v_r = v_r(\mathbf{R})$, $v_\theta = v_\theta(\mathbf{R})$, and $v_\varphi = v_\varphi(\mathbf{R})$. We use the symbol “ $\nabla|_{\mathbf{v}}$ ” to replace “ ∇ ” in Eq. (1) to stress that \mathbf{v} is fixed when calculating the spatial derivatives. Thus, Eq. (1) is rewritten as

$$\partial_t f + \mathbf{v} \cdot \nabla|_{\mathbf{v}} f = -\frac{1}{\tau} (f - f^{eq}). \quad (4)$$

According to the definition (3),

$$\nabla|_{\mathbf{v}} f = \nabla|_{v_r, v_\theta, v_\varphi} f + \nabla v_r \frac{\partial f}{\partial v_r} + \nabla v_\theta \frac{\partial f}{\partial v_\theta} + \nabla v_\varphi \frac{\partial f}{\partial v_\varphi}, \quad (5)$$

where

$$\nabla v_r = \frac{v_\theta}{r} \hat{\boldsymbol{\theta}} + \frac{v_\varphi}{r} \hat{\boldsymbol{\varphi}}, \quad (6)$$

$$\nabla v_\theta = -\frac{v_r}{r} \hat{\boldsymbol{\theta}} + \frac{v_\varphi \cos \theta}{r \sin \theta} \hat{\boldsymbol{\varphi}}, \quad (7)$$

$$\nabla v_\varphi = -\left(\frac{v_r}{r} + \frac{v_\theta \cos \theta}{r \sin \theta} \right) \hat{\boldsymbol{\varphi}}. \quad (8)$$

Substituting Eqs. (5)-(8) into Eq. (4) gives the Boltzmann equation in spherical coordinates,

$$\begin{aligned} & \partial_t f + \mathbf{v} \cdot \nabla|_{v_r, v_\theta, v_\varphi} f + \frac{v_\theta^2 + v_\varphi^2}{r} \frac{\partial f}{\partial v_r} + \left(\frac{v_\varphi^2 \cos \theta}{r \sin \theta} - \frac{v_r v_\theta}{r} \right) \frac{\partial f}{\partial v_\theta} - \left(\frac{v_r v_\varphi}{r} + \frac{v_\varphi v_\theta \cos \theta}{r \sin \theta} \right) \frac{\partial f}{\partial v_\varphi} \\ &= -\frac{1}{\tau} (f - f^{eq}). \end{aligned} \quad (9)$$

For macroscopic system with spherical symmetry, the distribution function f does not depend on the angles θ and φ , i.e.,

$$f = f(r, v_r, v_\theta, v_\varphi, t); \quad (10)$$

and f is invariant under the rotation in the subspace of (v_θ, v_φ) , i.e.,

$$f(r, v_r, v_\theta, v_\varphi, t) = f(r, v_r, v'_\theta, v'_\varphi, t) \quad (11)$$

when

$$v_\theta^2 + v_\varphi^2 = v'^2_\theta + v'^2_\varphi. \quad (12)$$

Now, we take $v'_\theta = v_\theta + dv_\theta$ and $v'_\varphi = v_\varphi + dv_\varphi$. From Eq.(11) we can get

$$f(r, v_r, v'_\theta, v'_\varphi, t) = f(r, v_r, v_\theta, v_\varphi, t) + \frac{\partial f}{\partial v_\theta} dv_\theta + \frac{\partial f}{\partial v_\varphi} dv_\varphi, \quad (13)$$

which gives

$$\frac{\partial f}{\partial v_\theta} dv_\theta + \frac{\partial f}{\partial v_\varphi} dv_\varphi = 0. \quad (14)$$

From Eq.(12) we can get

$$\frac{dv_\theta}{v_\phi} = -\frac{dv_\phi}{v_\theta}. \quad (15)$$

So,

$$\left(v_\theta \frac{\partial f}{\partial v_\varphi} - v_\varphi \frac{\partial f}{\partial v_\theta} \right) = 0. \quad (16)$$

Using the conditions, (10) and (16), in Eq. (9) gives

$$\partial_t f + \mathbf{v} \cdot \nabla|_{v_r, v_\theta, v_\varphi} f + \left(\frac{v_\theta^2 + v_\varphi^2}{r} \frac{\partial f}{\partial v_r} - \frac{v_r v_\theta}{r} \frac{\partial f}{\partial v_\theta} - \frac{v_r v_\varphi}{r} \frac{\partial f}{\partial v_\varphi} \right) = -\frac{1}{\tau} (f - f^{eq}). \quad (17)$$

It is clear that the term

$$\left(\frac{v_\theta^2 + v_\varphi^2}{r} \frac{\partial f}{\partial v_r} - \frac{v_r v_\theta}{r} \frac{\partial f}{\partial v_\theta} - \frac{v_r v_\varphi}{r} \frac{\partial f}{\partial v_\varphi} \right)$$

plays a similar role of the “force term” in the Boltzmann equation in Cartesian coordinates. It creates the divergence or convergence effects in the flow system. As the first step, here we consider the simplest case where the thermodynamic nonequilibrium effects resulted from the pure geometric effects are much weaker than those resulted from other kinds of contributions. In such a case, we can use the approximation, $f = f^{eq}$, when calculating the “force term”. Such a treatment is reasonable when the flow behaviors under consideration are not close to the spherical center. If further use the macroscopic condition, $u_\theta = u_\varphi = 0$, for spherical symmetry, the final Boltzmann equation for the flow system with spherical symmetry becomes,

$$\partial_t f + v_r \frac{\partial f}{\partial r} + \left[\frac{v_r v_\theta^2}{rT} + \frac{v_r v_\varphi^2}{rT} - \frac{(v_\theta^2 + v_\varphi^2)(v_r - u_r)}{rT} \right] f^{eq} = -\frac{1}{\tau} (f - f^{eq}). \quad (18)$$

2.2. Hydrodynamic model

The Navier-Stokes equations in Cartesian coordinates read

$$\frac{\partial \rho}{\partial t} + \frac{\partial(\rho u_\alpha)}{\partial x_\alpha} = 0, \quad (19a)$$

$$\frac{\partial(\rho u_\alpha)}{\partial t} + \frac{\partial(\rho u_\alpha u_\beta)}{\partial x_\beta} + \frac{\partial P \delta_{\alpha\beta}}{\partial x_\beta} = \frac{\partial \sigma_{\alpha\beta}}{\partial x_\beta}, \quad (19b)$$

$$\frac{\partial}{\partial t} (\rho e + \frac{1}{2} \rho u^2) + \frac{\partial}{\partial x_\alpha} [u_\alpha (\rho e + \frac{1}{2} \rho u^2 + P)] = \frac{\partial}{\partial x_\alpha} [Q_\alpha + u_\beta \sigma_{\alpha\beta}]. \quad (19c)$$

In the left-hand side of Eqs. (19a)- (19c), ρ , \mathbf{u} , $P = \rho RT$, $\rho e = (D + n) RT/2$, T , $\gamma = (D + n + 2) / (D + n)$ are the hydrodynamic density, flow velocity, pressure, internal energy, temperature and specific-heat ratio, respectively. $\alpha = x, y, \text{ or } z$. $u^2 = \mathbf{u} \cdot \mathbf{u}$. D is the space dimension and n is the number of extra degrees of freedom. In the right-hand side of Eqs. (19b)- (19c),

$$\sigma_{\alpha\beta} = \mu \left[\frac{\partial u_\beta}{\partial r_\alpha} + \frac{\partial u_\alpha}{\partial r_\beta} - \left(\frac{2}{D} - \lambda \right) \frac{\partial u_\gamma}{\partial r_\gamma} \delta_{\alpha\beta} \right] \quad (20)$$

is the viscous stress and

$$Q_\alpha = \kappa \frac{\partial e}{\partial r_\alpha} \quad (21)$$

is the heat flux. The two parameters, μ and λ are coefficient of viscosity and the parameter, κ is the coefficient of heat conductivity. $e = DRT/2$ is the translational internal energy. It is clear that $P = 2\rho e/D$. When the viscosities and

heat conductivity vanish, the hydrodynamic equations, (19a) - (19c), become the Euler equations.

2.3. From kinetic to hydrodynamic model

The Chapman-Enskog multiscale analysis shows that, the Navier-Stokes equations, (19a) - (19c), are the set of hydrodynamic equations from the Boltzmann BGK equation, (1), when only the first order terms in Knudsen number are taken into account. Among the infinite number of velocity kinetic moment relations of f^{eq} , only the following seven,

$$\int \int f^{eq} d\mathbf{v}d\boldsymbol{\eta} = \rho, \quad (22a)$$

$$\int \int f^{eq} v_\alpha d\mathbf{v}d\boldsymbol{\eta} = \rho u_\alpha, \quad (22b)$$

$$\int \int f^{eq} (v^2 + \eta^2) d\mathbf{v}d\boldsymbol{\eta} = 2\rho \left(\frac{D+n}{D} e + \frac{u^2}{2} \right), \quad (22c)$$

$$\int \int f^{eq} v_\alpha v_\beta d\mathbf{v}d\boldsymbol{\eta} = P \delta_{\alpha\beta} + \rho u_\alpha u_\beta, \quad (22d)$$

$$\int \int f^{eq} (v^2 + \eta^2) v_\alpha d\mathbf{v}d\boldsymbol{\eta} = 2\rho \left(\frac{D+n+2}{D} e + \frac{u^2}{2} \right) u_\alpha, \quad (22e)$$

$$\int \int f^{eq} v_\alpha v_\beta v_\chi d\mathbf{v}d\boldsymbol{\eta} = \rho RT (u_\alpha \delta_{\beta\chi} + u_\beta \delta_{\alpha\chi} + u_\chi \delta_{\alpha\beta}) + \rho u_\alpha u_\beta u_\chi, \quad (22f)$$

$$\int \int f^{eq} (v^2 + \eta^2) v_\alpha v_\beta d\mathbf{v}d\boldsymbol{\eta} = \frac{4}{D} \rho e \left(\frac{D+n+2}{D} e + \frac{u^2}{2} \right) \delta_{\alpha\beta} + 2\rho u_\alpha u_\beta \left(\frac{D+n+4}{D} e + \frac{u^2}{2} \right), \quad (22g)$$

are needed in the Chapman-Enskog analysis, where $\boldsymbol{\eta}$ is a parameter describing the fluctuating velocity in the n extra degrees of freedom, $\eta^2 = \boldsymbol{\eta} \cdot \boldsymbol{\eta}$, and

$$f^{eq}(\mathbf{v}) = \rho \left(\frac{1}{2\pi RT} \right)^{(D+n)/2} \exp \left[-\frac{(\mathbf{v} - \mathbf{u})^2 + \eta^2}{2RT} \right]. \quad (23)$$

The Chapman-Enskog analysis gives the following constitutive relations for the Navier-Stokes model, (19a) - (19c).

$$\mu = \frac{2}{D}\rho e\tau, \lambda = \frac{D+n-2}{D+n}, k = \frac{2(D+n+2)}{D(D+n)}\rho e\tau.$$

Under the spherical symmetry, the Navier-Stokes equations read

$$\begin{aligned} \partial_t \rho + \left(\partial_r + \frac{2}{r}\right)(\rho u) &= 0, \\ \partial_t u + u\partial_r u + \frac{1}{\rho}\partial_r p &= \frac{4}{\rho r}\mu\left(\partial_r u - \frac{u}{r}\right) - \frac{1}{\rho}\partial_r \left[\mu(1-\lambda)\left(\partial_r + \frac{2}{r}\right)u - 2\mu\partial_r u\right], \\ \partial_t e + u\partial_r e + \frac{p}{\rho} \left[\left(\partial_r + \frac{2}{r}\right)u\right] \\ &= \frac{1}{\rho}\left(\partial_r + \frac{2}{r}\right)(k\partial_r T) + \frac{2\mu}{\rho} \left[(\partial_r u)^2 + 2\left(\frac{u}{r}\right)^2\right] - \frac{1}{\rho}\mu(1-\lambda) \left[\left(\partial_r + \frac{2}{r}\right)u\right]^2 \end{aligned} \quad (24)$$

which can be recovered from the kinetic model (18). It should be stressed that the set of kinetic moment relations, (22a)-(22g), keep exactly the same form when being transferred from the (v_x, v_y, v_z) coordinates to the $(v_r, v_\theta, v_\varphi)$ coordinates, in this work, when using velocity kinetic moment relations, $v_\alpha = v_r, v_\theta, v_\varphi$.

2.4. Measurements of nonequilibrium effects

The Chapman-Enskog multiscale analysis tells that, as the simplest hydrodynamic model of fluid system, the Euler equations ignore completely the Thermodynamic Non-Equilibrium (TNE) behavior. The Navier-Stokes equations describe the TNE behavior via the terms in viscosity and heat conductivity. The Euler model works successfully when we consider the fluid system in a time scale t_0 which is large enough compared with thermodynamic relaxation time τ . Besides the normal high speed compressible flows, the Euler model works also for solid materials under strong shock. From the mechanical side, compared with the shocking strength, the material strength, for example, the yield, and viscous stress are negligible. Consequently, the Euler model works better with increasing the shock strength. From the side of time scales, when we study the shocking procedure, the time scale t_0 used is generally small enough compared

with the time scale t_h for heat conduction and large enough compared with the thermodynamic relaxation time τ . In other words, during the time interval under investigation, the heat conduction does not have time to occur significantly and consequently its effects are negligible. For the objective system where the thermodynamic relaxation time τ is fixed, if we decrease the observing time scale t_0 , we find more TNE effects. The Boltzmann kinetic model can be used to investigate both the hydrodynamic and thermodynamic behaviors.

Following the seven moment relations, (22a)-(22g), used in recovering the Navier-Stokes equations, we define the following moments,

$$\mathbf{M}_0^*(f, \mathbf{v}) = \int \int f \, d\mathbf{v} d\boldsymbol{\eta}, \quad (25a)$$

$$\mathbf{M}_1^*(f, \mathbf{v}) = \int \int f \, \mathbf{v} d\mathbf{v} d\boldsymbol{\eta}, \quad (25b)$$

$$\mathbf{M}_{2,0}^*(f, \mathbf{v}) = \int \int f \, (\mathbf{v} \cdot \mathbf{v} + \eta^2) \, d\mathbf{v} d\boldsymbol{\eta}, \quad (25c)$$

$$\mathbf{M}_2^*(f, \mathbf{v}) = \int \int f \, \mathbf{v} \mathbf{v} d\mathbf{v} d\boldsymbol{\eta}, \quad (25d)$$

$$\mathbf{M}_{3,1}^*(f, \mathbf{v}) = \int \int f \, (\mathbf{v} \cdot \mathbf{v} + \eta^2) \, \mathbf{v} d\mathbf{v} d\boldsymbol{\eta}, \quad (25e)$$

$$\mathbf{M}_3^*(f, \mathbf{v}) = \int \int f \, \mathbf{v} \mathbf{v} \mathbf{v} d\mathbf{v} d\boldsymbol{\eta}, \quad (25f)$$

$$\mathbf{M}_{4,2}^*(f, \mathbf{v}) = \int \int f \, (\mathbf{v} \cdot \mathbf{v} + \eta^2) \, \mathbf{v} \mathbf{v} d\mathbf{v} d\boldsymbol{\eta}, \quad (25g)$$

where \mathbf{M}_n^* means a n -th order tensor and $\mathbf{M}_{m,n}^*$ means a n -th-order tensor contracted from a m -th order tensor. For the case of central moments, the variable \mathbf{v} is replaced with $\mathbf{v}^* = (\mathbf{v} - \mathbf{u})$. It is clear \mathbf{M}_0^* and $\mathbf{M}_{2,0}^*$ are scalars. Each of them has only 1 component. \mathbf{M}_1^* and $\mathbf{M}_{3,1}^*$ are vectors. Each of them has 2 independent components in 2-dimensional case or 3 independent components in 3-dimensional case. \mathbf{M}_2^* and $\mathbf{M}_{4,2}^*$ are 2nd order tensors. Each of them has

3 independent components in 2-dimensional case or 6 independent components in 3-dimensional case. \mathbf{M}_3^* is 3rd tensor and has 4 independent components in 2-dimensional case or 10 independent components in 3-dimensional case. Therefore, the constraints, (22a) - (22g), are in fact 16 linear equations in f^{eq} in 2-dimensional case and 30 linear equations in f^{eq} in 3-dimensional case. We further define

$$\Delta_{m,n}^*(\mathbf{v}) = \mathbf{M}_{m,n}^*(f, \mathbf{v}) - \mathbf{M}_{m,n}^*(f^{eq}, \mathbf{v}). \quad (26)$$

It is clear that $\Delta_0^*(\mathbf{v}) = \mathbf{0}$, $\Delta_1^*(\mathbf{v}) = \mathbf{0}$ and $\Delta_{2,0}^*(\mathbf{v}) = \mathbf{0}$, which is due to the mass, momentum and energy conservations. Except for the three, the quantity $\Delta_{m,n}^*(\mathbf{v})$ works as a measure for the deviation of the system from its thermodynamic equilibrium. The information of flow velocity \mathbf{u} is taken into account in the definition (26). Similarly,

$$\Delta_{m,n}^*(\mathbf{v}^*) = \mathbf{M}_{m,n}^*(f, \mathbf{v}^*) - \mathbf{M}_{m,n}^*(f^{eq}, \mathbf{v}^*). \quad (27)$$

Except for $\Delta_0^*(\mathbf{v}^*)$, $\Delta_1^*(\mathbf{v}^*)$ and $\Delta_{2,0}^*(\mathbf{v}^*)$, the quantity $\Delta_{m,n}^*(\mathbf{v}^*)$ works as a measure for the deviation of the system from its thermodynamic equilibrium, where only the thermal fluctuations of the molecules are considered.

3. Discrete Boltzmann models for systems with spherical symmetry

There are two key techniques in constructing DBM with force terms. The first is to calculate the velocity derivative of f , $\partial f / \partial \mathbf{v}$, before discretizing the particle velocity space. As the first step, one can consider the case where f can be approximated by f^{eq} in the force term. The second is to write the discrete equilibrium distribution function, f_i^{eq} , as a function of the discrete velocities, where i is the index of the discrete velocity.

For constructing the DBM for systems with spherical symmetry, we use Eq. (18). We have

$$\partial_t f_i + v_{ir} \frac{\partial f_i}{\partial r} + \left[\frac{v_{ir} v_{i\theta}^2}{rT} + \frac{v_{ir} v_{i\varphi}^2}{rT} - \frac{(v_{i\theta}^2 + v_{i\varphi}^2)(v_{ir} - u)}{rT} \right] f_i^{eq} = -\frac{1}{\tau} (f_i - f_i^{eq}). \quad (28)$$

where f_i (f_i^{eq}) is the discrete (equilibrium) distribution function; v_i is the i -th discrete velocity, $i = 1, \dots, N$; N is the total number of the discrete velocity.

The fundamental requirement for a DBM is that it should recover the same set of hydrodynamic equations as those given by the original continuous Boltzmann equation. The Chapman-Enskog multiscale analysis shows that, only if the seven moment relations, (22a)-(22g), can be calculated equally in the summation form as below,

$$\rho = \sum_{i=1}^N f_i^{eq} = \sum_{i=1}^N f_i, \quad (29a)$$

$$\rho u_\alpha = \sum_{i=1}^N f_i^{eq} v_{i\alpha} = \sum_{i=1}^N f_i v_{i\alpha}, \quad (29b)$$

$$2\rho \left(\frac{D+n}{D} e + \frac{u^2}{2} \right) = \sum_{i=1}^N f_i^{eq} (v_i^2 + \eta_i^2) = \sum_{i=1}^N f_i (v_i^2 + \eta_i^2), \quad (29c)$$

$$P\delta_{\alpha\beta} + \rho u_\alpha u_\beta = \sum_{i=1}^N f_i^{eq} v_{i\alpha} v_{i\beta}, \quad (29d)$$

$$2\rho \left(\frac{D+n+2}{D} e + \frac{u^2}{2} \right) u_\alpha = \sum_{i=1}^N f_i^{eq} (v_i^2 + \eta_i^2) v_{i\alpha}, \quad (29e)$$

$$\rho RT (u_\alpha \delta_{\beta\chi} + u_\beta \delta_{\alpha\chi} + u_\chi \delta_{\alpha\beta}) + \rho u_\alpha u_\beta u_\chi = \sum_{i=1}^N f_i^{eq} v_{i\alpha} v_{i\beta} v_{i\chi}, \quad (29f)$$

$$\frac{4}{D} \rho e \left(\frac{D+n+2}{D} e + \frac{u^2}{2} \right) \delta_{\alpha\beta} + 2\rho u_\alpha u_\beta \left(\frac{D+n+4}{D} e + \frac{u^2}{2} \right) = \sum_{i=1}^N f_i^{eq} (v_i^2 + \eta_i^2) v_{i\alpha} v_{i\beta}, \quad (29g)$$

Navier-Stokes model, (19a) - (19c), can be recovered from the discrete Boltzmann model,(28). Following the same idea as in the definitions, (25a) - (25g), we define the following moments of the discrete distribution function f_i ,

$$\mathbf{M}_0(f_i, \mathbf{v}_i) = \sum_{i=1}^N f_i, \quad (30a)$$

$$\mathbf{M}_1(f_i, \mathbf{v}_i) = \sum_{i=1}^N f_i \mathbf{v}_i, \quad (30b)$$

$$\mathbf{M}_{2,0}(f_i, \mathbf{v}_i) = \sum_{i=1}^N f_i (\mathbf{v}_i \cdot \mathbf{v}_i + \eta_i^2), \quad (30c)$$

$$\mathbf{M}_2(f_i, \mathbf{v}_i) = \sum_{i=1}^N f_i \mathbf{v}_i \mathbf{v}_i, \quad (30d)$$

$$\mathbf{M}_{3,1}(f_i, \mathbf{v}_i) = \sum_{i=1}^N f_i (\mathbf{v}_i \cdot \mathbf{v}_i + \eta_i^2) \mathbf{v}_i, \quad (30e)$$

$$\mathbf{M}_3(f_i, \mathbf{v}_i) = \sum_{i=1}^N f_i \mathbf{v}_i \mathbf{v}_i \mathbf{v}_i, \quad (30f)$$

$$\mathbf{M}_{4,2}(f_i, \mathbf{v}_i) = \sum_{i=1}^N f_i (\mathbf{v}_i \cdot \mathbf{v}_i + \eta_i^2) \mathbf{v}_i \mathbf{v}_i, \quad (30g)$$

where \mathbf{M}_n means a n -th order tensor and $\mathbf{M}_{m,n}$ means a n -th-order tensor contracted from a m -th order tensor. For the case of central moments, the variable \mathbf{v} is replaced with $\mathbf{v}^* = (\mathbf{v} - \mathbf{u})$. The constraints, (29a) - (29g), are in fact 16 linear equations in f_i^{eq} in 2-dimensional case and 30 linear equations in f_i^{eq} in 3-dimensional case. Following the same idea as in the definitions, (26) - (27), we further define

$$\Delta_{m,n}(\mathbf{v}_i) = \mathbf{M}_{m,n}(f_i, \mathbf{v}_i) - \mathbf{M}_{m,n}(f_i^{eq}, \mathbf{v}_i). \quad (31)$$

$$\Delta_{m,n}(\mathbf{v}_i^*) = \mathbf{M}_{m,n}(f_i, \mathbf{v}_i^*) - \mathbf{M}_{m,n}(f_i^{eq}, \mathbf{v}_i^*). \quad (32)$$

Except for Δ_0 , Δ_1 and $\Delta_{2,0}$, the quantity $\Delta_{m,n}$ works as a measure for the deviation of the system from its thermodynamic equilibrium.

The constraints, (29a) - (29g) can also be rewritten as

$$\hat{\mathbf{f}}^{eq} = \mathbf{C} \mathbf{f}^{eq} \quad (33)$$

where $\hat{\mathbf{f}}^{eq} = [\hat{f}_k^{eq}]^T$ and $\mathbf{f}^{eq} = [f_k^{eq}]^T$ are column vectors with $k = 1, 2, \dots, N$, \mathbf{C} is $N \times N$ matrix whose components are determined by \mathbf{v}_i if the parameter η_i is fixed. It is clear that

$$\mathbf{f}^{eq} = \mathbf{C}^{-1} \hat{\mathbf{f}}^{eq}. \quad (34)$$

Obviously, the choosing of the DVM must ensure the existence of \mathbf{C}^{-1} . The specific choice of the DVM depends on the compromise among the following several points: (i) numerical efficiency, (ii) numerical stability, (iii) local symmetry of relevant kinetic moments. We work in the frame where the particle mass $m = 1$ and the constant $R = 1$.

If we require the DBM to recover the Navier-Stokes equations in the continuum limit, the DBM needs a DVM with 3 dimensions.

3.1. Case with $\gamma = 5/3$

We first consider the simple case where ratio of specific rates is fixed, $\gamma = 5/3$. We set $\eta_i = 0$ and $n = 0$ in constraint (29g). Among the seven moment constraints, (29a) - (29g), only five are independent. We do not use the constraints (29c) and (29e). The five independent constraints can be rewritten as 26 independent linear equations in f_i^{eq} . Now, we fix the components \hat{f}_k^{eq} of $\hat{\mathbf{f}}^{eq}$. Here $N = 26$.

From the constraint (29a), we have $\hat{f}_1^{eq} = \rho$. From the constraint (29b), we have $\hat{f}_2^{eq} = \rho u_r$, $\hat{f}_3^{eq} = \rho u_\theta$, $\hat{f}_4^{eq} = \rho u_\varphi$. From the constraint (29d), we have $\hat{f}_5^{eq} = P + \rho u_r^2$, $\hat{f}_6^{eq} = \rho u_r u_\theta$, $\hat{f}_7^{eq} = \rho u_r u_\varphi$, $\hat{f}_8^{eq} = P + \rho u_\theta^2$, $\hat{f}_9^{eq} = \rho u_\theta u_\varphi$, $\hat{f}_{10}^{eq} = P + \rho u_\varphi^2$. From the constraint (29f), we have $\hat{f}_{11}^{eq} = \rho [T(3u_r) + u_r^3]$, $\hat{f}_{12}^{eq} = \rho (Tu_\theta + u_r^2 u_\theta)$, $\hat{f}_{13}^{eq} = \rho (Tu_\varphi + u_r^2 u_\varphi)$, $\hat{f}_{14}^{eq} = \rho (Tu_r + u_r u_\theta^2)$, $\hat{f}_{15}^{eq} = \rho (u_r u_\theta u_\varphi)$, $\hat{f}_{16}^{eq} = \rho (Tu_r + u_r u_\varphi^2)$, $\hat{f}_{17}^{eq} = \rho [T(3u_\theta) + u_\theta^3]$, $\hat{f}_{18}^{eq} = \rho [Tu_\varphi + u_\theta^2 u_\varphi]$, $\hat{f}_{19}^{eq} = \rho [Tu_\theta + u_\varphi^2 u_\theta]$, $\hat{f}_{20}^{eq} = \rho [T(3u_\varphi) + u_\varphi^3]$. From the constraint (29g), we have $\hat{f}_{21}^{eq} = \rho T(5T + u^2) + \rho u_r^2(7T + u^2)$, $\hat{f}_{22}^{eq} = \rho u_r u_\theta(7T + u^2)$, $\hat{f}_{23}^{eq} = \rho u_r u_\varphi(7T + u^2)$, $\hat{f}_{24}^{eq} = \rho T(5T + u^2) + \rho u_\theta^2(7T + u^2)$, $\hat{f}_{25}^{eq} = \rho u_\theta u_\varphi(7T + u^2)$, $\hat{f}_{26}^{eq} = \rho T(5T + u^2) + 2\rho u_\varphi^2(7T + u^2)$.

Since the system is spherically symmetric in macroscopic scale, $u_\theta = u_\varphi = 0$ and $u^2 = u_r^2$ in the above expressions for $\hat{\mathbf{f}}^{eq} = [\hat{f}_1^{eq}, \hat{f}_2^{eq}, \dots, \hat{f}_N^{eq}]^T$.

The components of the matrix $\mathbf{C} = [\mathbf{C}_k] = [C_{ki}]$ should be fixed in the same sequence, where $k = 1, 2, \dots, 26$ and $i = 1, 2, \dots, 26$. From the constraint (29a), we have $C_{1i} = 1$. From the constraint (29b), we have $C_{2i} = v_{ir}$, $C_{3i} = v_{i\theta}$, $C_{4i} = v_{i\varphi}$. From the constraint (29d), we have $C_{5i} = v_{ir}^2$, $C_{6i} = v_{ir}v_{i\theta}$, $C_{7i} = v_{ir}v_{i\varphi}$, $C_{8i} = v_{i\theta}^2$, $C_{9i} = v_{i\theta}v_{i\varphi}$, $C_{10i} = v_{i\varphi}^2$. From the constraint (29f), we have $C_{11i} = v_{ir}^3$, $C_{12i} = v_{ir}^2v_{i\theta}$, $C_{13i} = v_{ir}^2v_{i\varphi}$, $C_{14i} = v_{ir}v_{i\theta}^2$, $C_{15i} = v_{ir}v_{i\theta}v_{i\varphi}$, $C_{16i} = v_{ir}v_{i\varphi}^2$, $C_{17i} = v_{i\theta}^3$, $C_{18i} = v_{i\theta}^2v_{i\varphi}$, $C_{19i} = v_{i\theta}v_{i\varphi}^2$, $C_{20i} = v_{i\varphi}^3$. From the constraint (29g), we have $C_{21i} = (v_{ir}^2 + v_{i\theta}^2 + v_{i\varphi}^2)v_{ir}^2$, $C_{22i} = (v_{ir}^2 + v_{i\theta}^2 + v_{i\varphi}^2)v_{ir}v_{i\theta}$, $C_{23i} = (v_{ir}^2 + v_{i\theta}^2 + v_{i\varphi}^2)v_{ir}v_{i\varphi}$, $C_{24i} = (v_{ir}^2 + v_{i\theta}^2 + v_{i\varphi}^2)v_{i\theta}^2$, $C_{25i} = (v_{ir}^2 + v_{i\theta}^2 + v_{i\varphi}^2)v_{i\theta}v_{i\varphi}$, $C_{26i} = (v_{ir}^2 + v_{i\theta}^2 + v_{i\varphi}^2)v_{i\varphi}^2$.

An example for the 3-Dimensional 26-Velocity(D3V26) DVM is as below,

$$\mathbf{v}_i = \begin{cases} (0, \pm 1, \pm 1) c_1 & i = 1, \dots, 4 \\ (\pm 1, 0, \pm 1) c_1 & i = 5, \dots, 8 \\ (\pm 1, \pm 1, 0) c_1 & i = 9, \dots, 12 \end{cases} \quad (35a)$$

$$\mathbf{v}_i = \begin{cases} (\pm 1, \pm 1, \pm 1) c_2 & i = 13, \dots, 20 \end{cases} \quad (35b)$$

$$\mathbf{v}_i = \begin{cases} (\pm 1, 0, 0) c_3 & i = 21, 22 \\ (0, \pm 1, 0) c_3 & i = 23, 24 \\ (0, 0, \pm 1) c_3 & i = 25, 26 \end{cases} \quad (35c)$$

The schematic of the discrete velocity model is shown in Figure 2. The expressions for the inverse of the matrix \mathbf{C} , $\mathbf{C}^{-1} = [\mathbf{C}_k^{-1}]$, can be easily obtained by using the software, MatLab, then a specific example of the DVM is formulated.

Up to this step, a specific discretization of the velocity space has been performed. Consequently, the DBM for system with spherical symmetry and $\gamma = 5/3$ has been constructed. The spatial and temporal derivatives of the distribution function in the kinetic model can be calculated in the normal way. If we are not interested in the extra degrees of freedom other than the translational, the formulated DBM can be used to study the hydrodynamic and the thermodynamic behaviors of the compressible flow system. The computational domain in this work can be found in Figure 3 where the projection of computational domain in two-dimensional space is shown. In the rest of the article,

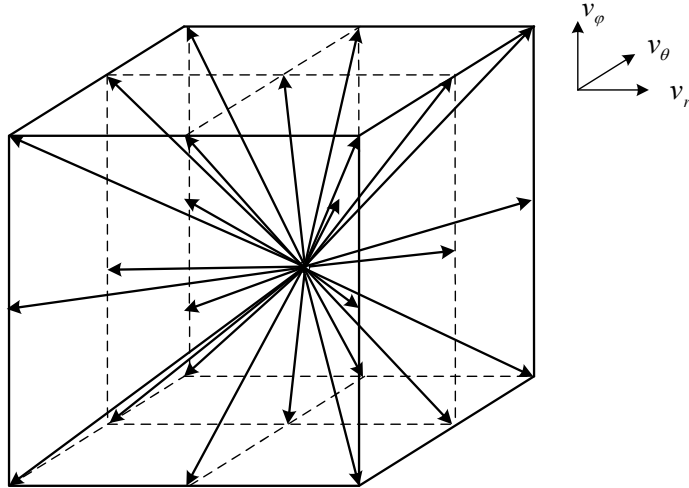


Figure 2: Schematic of the discrete velocity model (D3V26).

$r - r_0$ is used as the label of the space axis where r_0 is the distance between the computational domain and the centre of sphere.

Firstly, we simulate a Sod shock tube problem using the DBM where the “force term” in Eq. (28) does not exist. Such a test can be used to check the validity of the DVM. In addition, the case with “force term” vanished corresponds the case where the value of r_0 is so large that the geometric effects are negligible. The results are shown in Figure 4. The Riemann solutions are also plotted for comparison. The calculated results show that the new DVM (D3V26) is applicable and the new DBM model can capture the discontinuous interface.

Then, to check the geometric effects, two cases of propagating shock wave with Mach number $Ma = 1.5$ along the radial direction are simulated. In the first case the shock wave propagates outward so that the divergence makes effects. Several cases with different values of r_0 are simulated. The results are shown in Figure 5(a). For easy understanding, the three dimensional contour maps of hydrodynamic quantities at a certain time for the case with $r_0 = 0.5$ are given in Figure 6. Figure 5(a) shows the variation of position of wavefront with time. From the figure, we can find that the propagation speed of shock wave

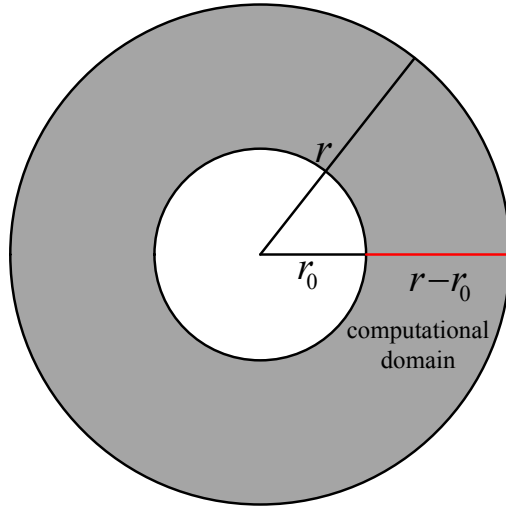


Figure 3: Schematic of the computational domain (gray area).

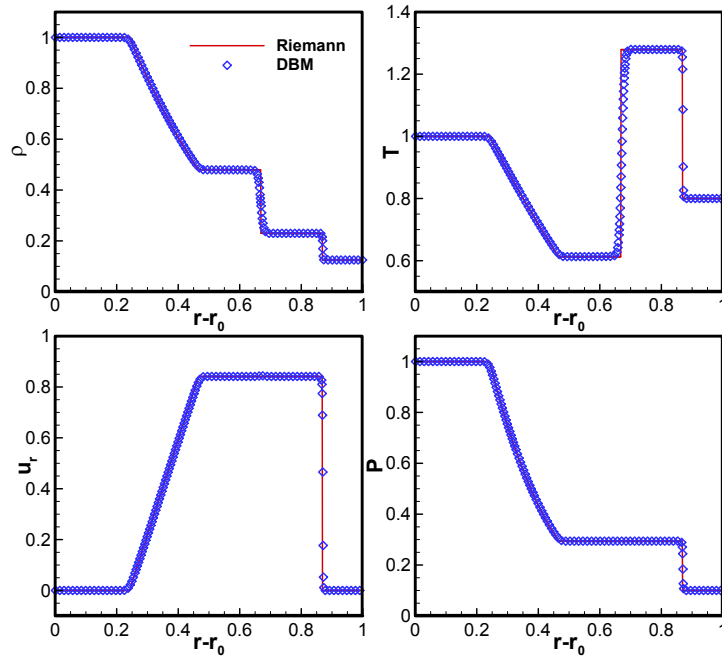


Figure 4: Profile of macroquantities for Sob shock tube with $\gamma = 5/3$.

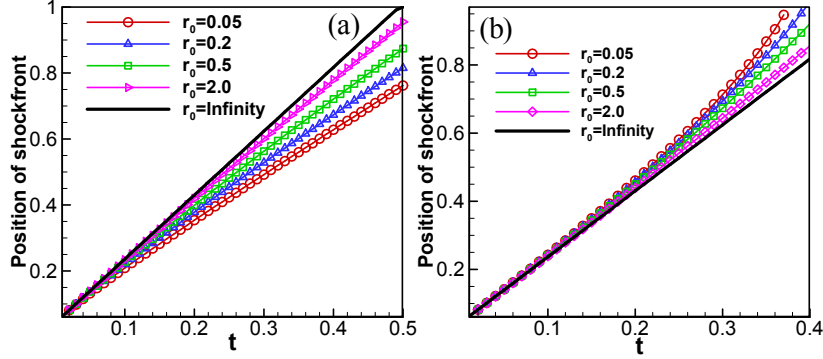


Figure 5: The position of shock wavefront versus time for the case with $\gamma = 5/3$. (a) Shock wave propagates outward (explosion). (b) Shock wave propagates inward (implosion).

decreases with time due to the divergence effect. Besides, the smaller r_0 has a faster decrease of propagation speed. The second case is that the shock wave propagates inward so the convergence effect plays a role. Figure 5(b) shows the variation of position of wavefront with time. The propagation speed of shock wave increases with time due to the convergence effect, and the smaller r_0 has a faster increase of propagation speed.

The above simulation results and analysis show that the new model can well describe the geometric effects of the flows with spherical symmetry.

3.2. Case with flexible γ

For the case with flexible ratio of specific heat γ , if we are interested only in the hydrodynamic behaviors, we can use the simulation results of the DBM formulated in last subsection. Just get the number n of the extra degree of freedom using its relation to γ , then obtain the total internal energy E using its definition. If we are interested also in the thermodynamic nonequilibrium behavior, we need to continue the formulation of DBM.

To model the case with flexible γ , we resort to the parameter η to describe the contribution of extra degrees of freedom. The distribution function f with n extra degrees of freedom can be replaced by g and h , and the equilibrium

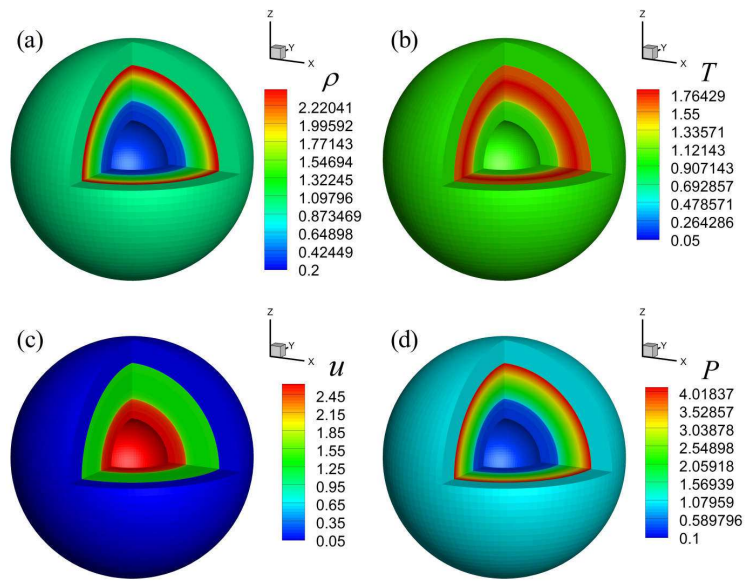


Figure 6: The contour maps of macroquantities for shock wave propagating outward for $r_0 = 0.5$ at $t = 0.9$. (a)Contour map of density, ρ . (b)Contour map of temperature, T . (c)Contour map of velocity, u . (d)Contour map of pressure, P .

distribution function f^{eq} in Eq.(23) is replaced by g^{eq} and h^{eq} , where

$$g = \int f d\boldsymbol{\eta}, \quad (36a)$$

$$h = \int f \eta^2 d\boldsymbol{\eta}, \quad (36b)$$

$$g^{eq} = \int f^{eq} d\boldsymbol{\eta}, \quad (36c)$$

$$h^{eq} = \int f^{eq} \eta^2 d\boldsymbol{\eta}. \quad (36d)$$

The functions g and g^{eq} recover to the f and f^{eq} when there is no extra degrees of freedom (i.e., $\gamma = 5/3$). The evolution equation of f in Eq.(18) becomes two evolution equations of g and h . They read

$$\partial_t g + v_r \frac{\partial g}{\partial r} + \left[\frac{v_r v_\theta^2}{rT} + \frac{v_r v_\varphi^2}{rT} - \frac{(v_\theta^2 + v_\varphi^2)(v_r - u_r)}{rT} \right] g^{eq} = -\frac{1}{\tau} (g - g^{eq}), \quad (37a)$$

$$\partial_t h + v_r \frac{\partial h}{\partial r} + \left[\frac{v_r v_\theta^2}{rT} + \frac{v_r v_\varphi^2}{rT} - \frac{(v_\theta^2 + v_\varphi^2)(v_r - u_r)}{rT} \right] h^{eq} = -\frac{1}{\tau} (h - h^{eq}). \quad (37b)$$

where

$$g^{eq}(\mathbf{v}) = \rho \left(\frac{1}{2\pi RT} \right)^{D/2} \exp \left[-\frac{(\mathbf{v} - \mathbf{u})^2}{2RT} \right], \quad (38a)$$

$$h^{eq} = \frac{nT}{2} g^{eq}. \quad (38b)$$

As a result, the f_i^{eq} solved before, for the case with $\gamma = 5/3$, can be used as g_i^{eq} here. The h_i^{eq} can be solved by

$$h_i^{eq} = \frac{nT}{2} g_i^{eq}. \quad (39)$$

In this case, the discretization of $\boldsymbol{\eta}$ does not need at all, and the moments in Eq.(30a)-(30g) are calculated by

$$\mathbf{M}_0(f_i, \mathbf{v}_i) = \sum_{i=1}^N g_i, \quad (40a)$$

$$\mathbf{M}_1(f_i, \mathbf{v}_i) = \sum_{i=1}^N g_i \mathbf{v}_i, \quad (40b)$$

$$\mathbf{M}_{2,0}(f_i, \mathbf{v}_i) = \sum_{i=1}^N [g_i(\mathbf{v}_i \cdot \mathbf{v}_i) + h_i], \quad (40c)$$

$$\mathbf{M}_2(f_i, \mathbf{v}_i) = \sum_{i=1}^N g_i \mathbf{v}_i \mathbf{v}_i, \quad (40d)$$

$$\mathbf{M}_{3,1}(f_i, \mathbf{v}_i) = \sum_{i=1}^N [g_i(\mathbf{v}_i \cdot \mathbf{v}_i) + h_i] \mathbf{v}_i, \quad (40e)$$

$$\mathbf{M}_3(f_i, \mathbf{v}_i) = \sum_{i=1}^N g_i \mathbf{v}_i \mathbf{v}_i \mathbf{v}_i, \quad (40f)$$

$$\mathbf{M}_{4,2}(f_i, \mathbf{v}_i) = \sum_{i=1}^N [g_i(\mathbf{v}_i \cdot \mathbf{v}_i) + h_i] \mathbf{v}_i \mathbf{v}_i, \quad (40g)$$

The constraints, (40a)-(40g), are 16 linear equations in 2-dimensional case and 30 linear equations equations in 3-dimensional case. The definitions of $\Delta_{m,n}(\mathbf{v}_i)$ and $\Delta_{m,n}(\mathbf{v}_i^*)$ in Eq.(31) and (32) still keep the same and work as a measure for the deviation of the system from its thermodynamic equilibrium. Up to this step, a DBM with D3V26 for system with flexible specific heat ratio γ has been formulated.

In order to test the flexibility of γ , Sod shock tube problems with two different values of γ are simulated. The specific heat ratio for one case is $\gamma = 1.4$ which means there are two extra degrees of freedom ($n = 2$), and the other case is $\gamma = 1.5$ which means there is only one extra degree of freedom ($n = 1$). First ignore the geometric effects. The results for the two cases are shown Figure 7 and Figure 8, respectively. The results are in well agreement with Riemann solutions which verifies the validity of the new model.

Then, a shock wave with $Ma = 3$ propagating along the radial direction is simulated for the case with $\gamma = 1.4$ (i.e., $n = 2$). Firstly, we assume that shock wave starts at infinity from the centre of sphere, so the “force term” in Eqs.(37a) and (37b) are negligible. The profiles of the macroquantities, including ρ , u , and P around wavefront at a certain time are shown in Figure 9(a). The macroquantities on the two sides of wavefront satisfy the Hugoniot relations of

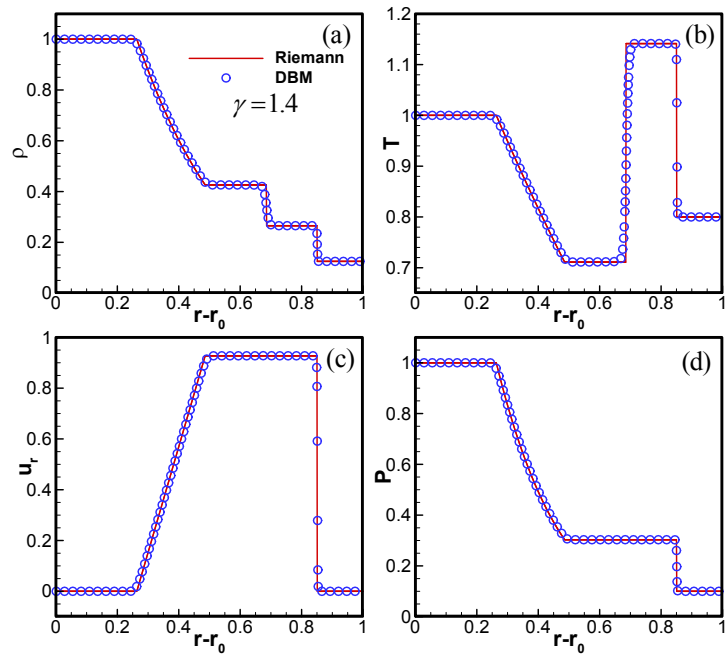


Figure 7: Profiles of macroquantities for Sob shock tube with $\gamma = 1.4$ ($n = 2$).

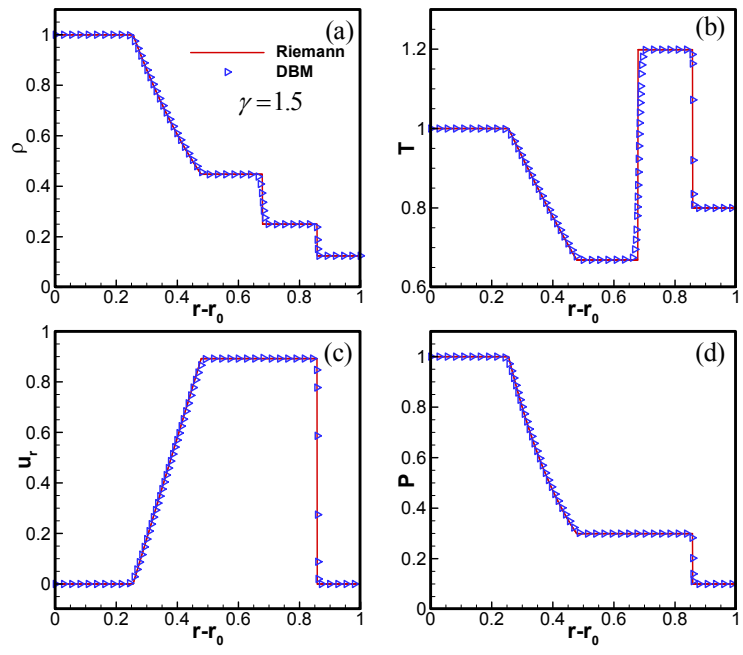


Figure 8: Profiles of macroquantities for Sob shock tube with $\gamma = 1.5$ ($n = 1$).

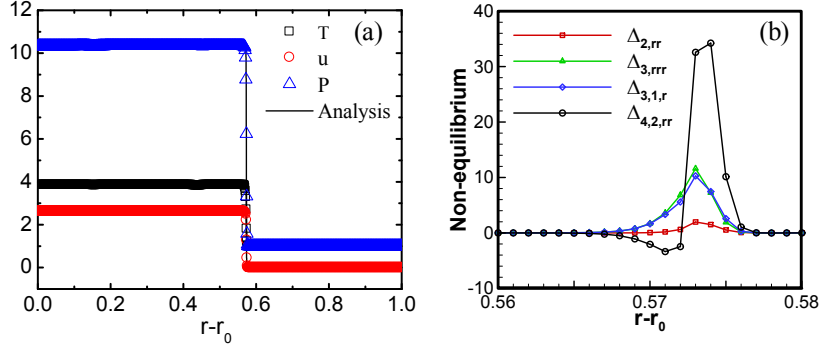


Figure 9: Profiles of macroquantities and non-equilibrium effects around shock wavefront for the case with $Ma = 3.0$ and $\gamma = 1.4$. (a) Profiles of ρ , u , and P . The symbols indicate the results of DBM and solid lines are solutions based on Hugoniot relations of shock wave. (b) Profiles of non-equilibrium effects around shock wavefront.

shock wave. The corresponding non-equilibrium quantities including $\Delta_{2,rr}(v_i)$, $\Delta_{3,rrr}(v_i)$, $\Delta_{3,1,r}(v_i)$, and $\Delta_{4,2,rr}(v_i)$ around the wavefront are plotted in Figure 9(b). Since the shock propagate along the radial direction, only one component in r direction is considered for each of the four kinds non-equilibrium quantities. From Figure 9(b), we can get the non-equilibrium characteristics from a different point of view, other than the viscous stress and heat flux, which can not be provided by the traditional Navier-Stokes equations.

Then the geometric effects are taken into account. Shock waves propagating outward and inward are both simulated. The evolutions of positions of wavefront are shown in Figures 10(a) and 10(b), respectively.

From Figure 10(a), it can be seen the shock wave has a constant propagation speed for $r_0 = \text{Infinity}$ which corresponds to the case in Figure 9. For the shock wave propagating outward, the propagation speed decrease with time, and the smaller r_0 has a faster decrease which indicates a stronger “force” caused by geometric effects. The shock wave propagating inward has a similar characteristics, except that the propagation speed increase with time due to the convergence effect.

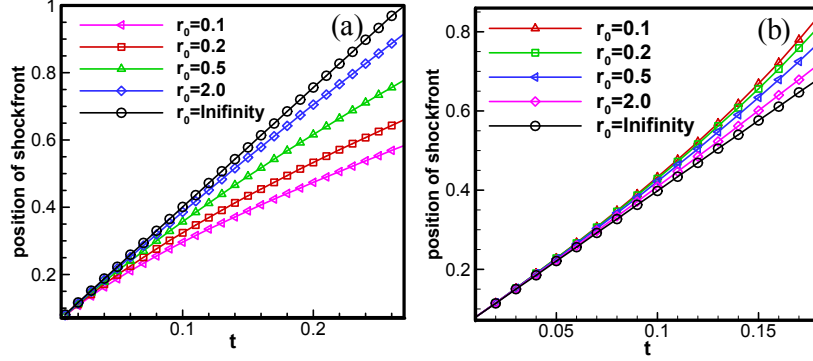


Figure 10: The position of shock wavefront versus time for the case with $\gamma = 1.4$. (a) Shock wave propagates outward. (b) Shock wave propagates inward.

3.3. Thermodynamic non-equilibrium characteristics in explosion and implosion

The non-equilibrium quantities around wavefront for the shock propagating outward (i.e., explosion), at a certain time, are plotted in Figure 11. In this case, the divergence effect plays the role of resistance force. It decreases the propagation speed and reduce the non-equilibrium strength. It can be found in Figure 11(b) that a smaller r_0 , which means a stronger divergence effect, may even change the direction of deviation from equilibrium state for $\Delta_{3,rrr}$.

It is interesting to have more discussions on the reasonability of the approximation $f = f^{eq}$ in treating with the term for pure geometric effects in Eq.(17). When the flow under consideration is not close to the spherical center, the error induced by the approximation when calculating the “force term” is relatively very small compared with the “convective term“. The comparison can be made in the moment space.

Firstly, the “force term” in moment space is defined as

$$\mathbf{M}_n^{Geo}(f) = \int \left(\frac{v_\theta^2 + v_\varphi^2}{r} \frac{\partial f}{\partial v_r} - \frac{v_r v_\theta}{r} \frac{\partial f}{\partial v_\theta} - \frac{v_r v_\varphi}{r} \frac{\partial f}{\partial v_\varphi} \right) \mathbf{v}^n d\mathbf{v}, \quad (41)$$

where the subscript n in $\mathbf{M}_n^{Geo}(f)$ indicates the n -th order moment. Then the error induced by the approximation $f = f^{eq}$ in the moment space is

$$\Delta_n^{Geo} = \mathbf{M}_n^{Geo}(f) - \mathbf{M}_n^{Geo}(f^{eq}), \quad (42)$$

Similarly, the convective term in the moment space is defined as

$$\mathbf{M}_n^{Con}(f) = \int (\mathbf{v} \cdot \nabla f) \mathbf{v}^n d\mathbf{v}. \quad (43)$$

The ratio $\Delta_n^{Geo}/M_n^{Con}(f)$ measures the relative error induced by $f = f^{eq}$ when calculating the “force term” with respect to the convective term. Since the density, momentum, and energy is the 0-th order, 1st order, and 2nd order moments, respectively, only the Δ_0^{Geo}/M_0^{Con} , $\Delta_{1,r}^{Geo}/M_{1,r}^{Con}$, and $\Delta_{2,0}^{Geo}/M_{2,0}^{Con}$ are investigated here. The subscript “2,0” indicates that $\Delta_{2,0}^{Geo}$ (or $M_{2,0}^{Con}$) is a 0-th order tensor (i.e., scalar) contracted from the 2nd order tensor. According to the definition of Δ_n^{Geo} and $\mathbf{M}_n^{Con}(f)$, we can get that

$$\frac{\Delta_0^{Geo}}{M_0^{Con}} = \frac{\int 2\frac{v_r}{r} (f - f^{eq}) d\mathbf{v}}{\int (\mathbf{v} \cdot \nabla f) d\mathbf{v}}, \quad (44)$$

$$\frac{\Delta_{1,r}^{Geo}}{M_{1,r}^{Con}} = \frac{\int \left(-\frac{v_\theta^2 + v_\varphi^2}{r} + 2\frac{v_r v_\theta}{r} + 2\frac{v_r v_\varphi}{r} \right) (f - f^{eq}) d\mathbf{v}}{\frac{\partial M_{2,rr}}{\partial r} + \frac{\partial M_{2,r\theta}}{\partial \theta} + \frac{\partial M_{2,r\varphi}}{\partial \varphi}}, \quad (45)$$

$$\frac{\Delta_{2,0}^{Geo}}{M_{2,0}^{Con}} = \frac{\int \left[\left(-2v_r \frac{v_\theta^2 + v_\varphi^2}{r} \right) + \left(\frac{v_r^3 + 3v_r v_\theta^2 + v_r v_\varphi^2}{r} \right) + \left(\frac{v_r^3 + v_r v_\theta^2 + 3v_r v_\varphi^2}{r} \right) \right] (f - f^{eq}) d\mathbf{v}}{\frac{\partial M_{3,1,r}}{\partial r} + \frac{\partial M_{3,1,\theta}}{\partial \theta} + \frac{\partial M_{3,1,\varphi}}{\partial \varphi}}. \quad (46)$$

It is obvious that Δ_0^{Geo}/M_0^{Con} is always equal to zero. Therefore, only the $\Delta_{1,r}^{Geo}/M_{1,r}^{Con}$ and $\Delta_{2,0}^{Geo}/M_{2,0}^{Con}$ are used to measure the relative error of “force term”. The profiles of $\Delta_{1,r}^{Geo}/M_{1,r}^{Con}$, $\Delta_{1,r}^{Geo}$, and $M_{1,r}^{Con}$ for the case with $r_0 = 0.1$ is shown in Figure 12(a). It can be seen that $\Delta_{1,r}^{Geo}$ is so small compared with $M_{1,r}^{Con}$ that it nearly can be ignored even for such a small r_0 . From the Figure 12(b) we can see the $\Delta_{2,0}^{Geo}$ is also nearly negligible compared with $M_{2,0}^{Con}$. Besides, with the increase of r_0 , the effects become weaker, the Δ_n^{Geo} is more negligible compared with M_n^{Con} , which is verified in Figure 13. From Figure 13 we can conclude that the error Δ_n^{Geo} is negligible compared with M_n^{Con} when $r_0 \geq 0.1$.

For the shock propagating inward, the non-equilibrium quantities at a certain time are shown in Figure 14. In this case, the convergence effect accelerates the propagation speed of the shock wave. So the non-equilibrium effects around

wavefront are also strengthened. A smaller r_0 corresponds to a stronger non-equilibrium. Unlike the shock propagating outward, no change of the direction for the deviation from thermodynamic equilibrium state is found.

The comparisons between the error caused by the approximation $f = f^{eq}$ when calculating the “force term” and the convective term are given in Figure 15 and Figure 16. The profiles of $\Delta_{1,r}^{Geo}/M_{1,r}^{Con}$, $\Delta_{1,r}^{Geo}$, and $M_{1,r}^{Con}$ for the case with $r_0 = 0.1$ is shown in Figure 15(a). It can be seen that $\Delta_{1,r}^{Geo}$ is so small compared with $M_{1,r}^{Con}$ that it nearly can be ignored even for such a small r_0 . From the Figure 15(b) we can see the $\Delta_{2,0}^{Geo}$ is also nearly negligible compared with $M_{2,0}^{Con}$. Besides, with the increase of r_0 , the effects become weaker, the Δ_n^{Geo} is more negligible compared with M_n^{Con} , which is verified in Figure 16. From Figure 16 we can conclude that the error Δ_n^{Geo} is negligible compared with M_n^{Con} when $r_0 \geq 0.1$ for the current implosion numerical experiment setup.

4. Conclusion and discussions

We present a theoretical framework for constructing DBM in spherical coordinates for the compressible flow systems with spherical symmetry. A key technique here is to use *local* Cartesian coordinates to describe the particle velocity. Thus, compared with the Boltzmann equation in Cartesian coordinates, the geometric effects, like the divergence and convergence, are treated as a “force term”. For such a system, even though the hydrodynamic model is one-dimensional, the DBM needs a discrete velocity model with 3 dimensions. A new scheme is introduced so that the DBM can use the same set of discrete velocities no matter the extra degrees of freedom are considered or not. We use 26 discrete velocities to formulate the DBM in Navier-Stokes level.

Besides recovering the hydrodynamic equations in the continuum limit, two key points for a DBM are as below: (i) in terms of the nonconserved moments, we can define two sets of measures for the deviation of the system from its thermodynamic equilibrium state, (ii) in the regimes where the system deviates from its thermodynamic equilibrium, the DBM may present more reasonable

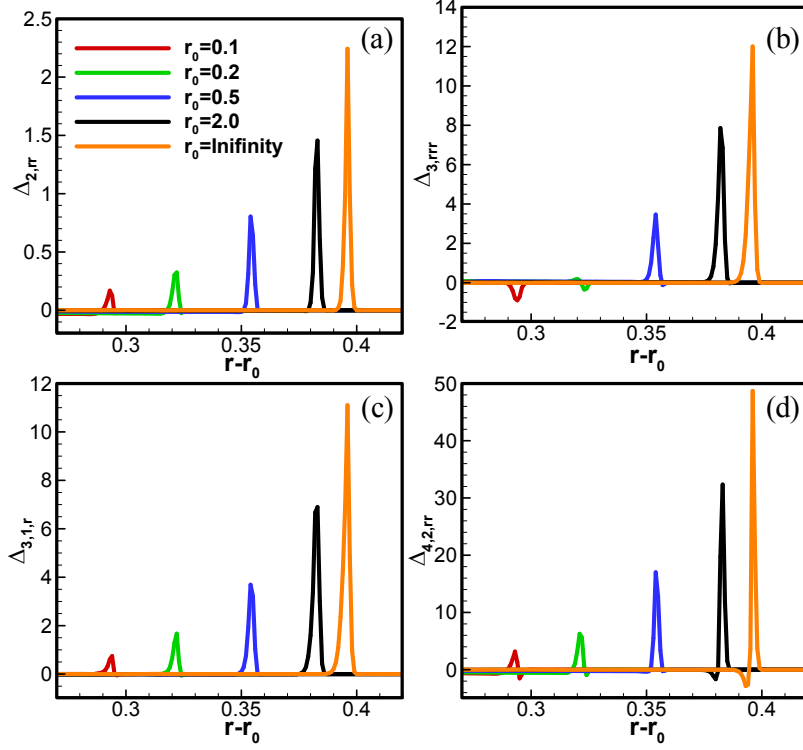


Figure 11: The non-equilibrium quantities around wavefront for explosion.

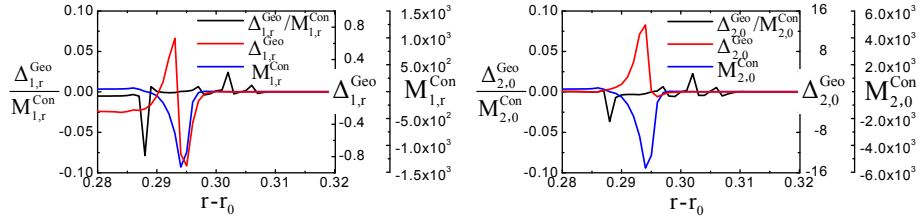


Figure 12: The profiles of (a) $\Delta_{1,r}^{Geo}/M_{1,r}^{Con}$, $\Delta_{1,r}^{Geo}$, and $M_{1,r}^{Con}$ and (b) $\Delta_{2,0}^{Geo}/M_{2,0}^{Con}$, $\Delta_{2,0}^{Geo}$, and $M_{2,0}^{Con}$ around the shock wave front for the case with $r_0 = 0.1$ (explosion).

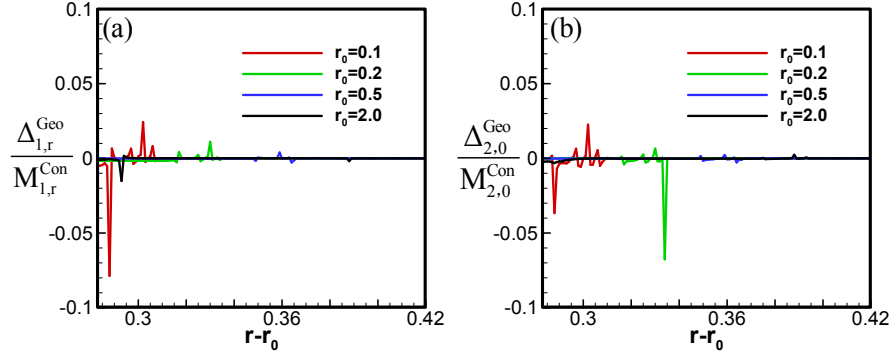


Figure 13: The profiles of (a) $\Delta_{1,r}^{Geo}/M_{1,r}^{Con}$ and (b) $\Delta_{2,0}^{Geo}/M_{2,0}^{Con}$ around the shock wave front for different cases (explosion).

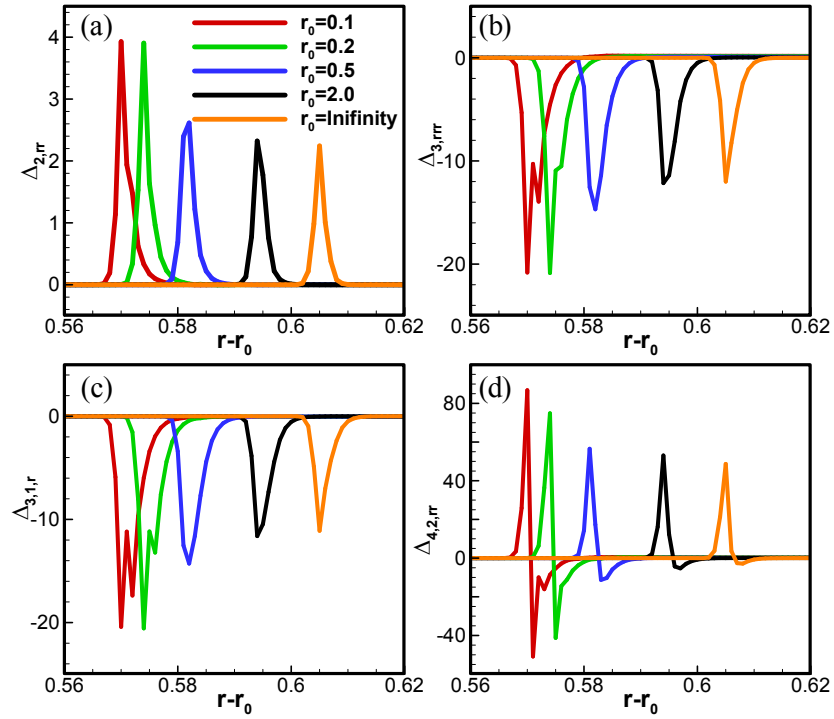


Figure 14: The non-equilibrium quantities around wavefront for implosion.

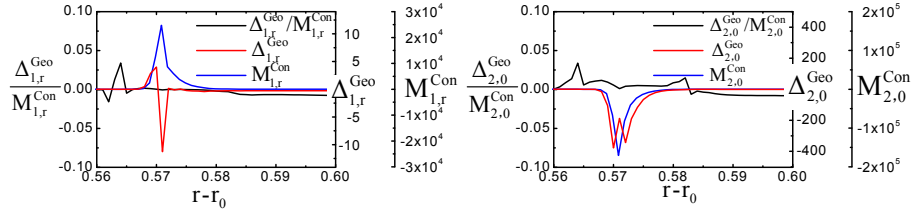


Figure 15: The profiles of (a) $\Delta_{1,r}^{Geo}/M_{1,r}^{Con}$, $\Delta_{1,r}^{Geo}$, and $M_{1,r}^{Con}$ and (b) $\Delta_{2,0}^{Geo}/M_{2,0}^{Con}$, $\Delta_{2,0}^{Geo}$, and $M_{2,0}^{Con}$ around the shock wave front for the case with $r_0 = 0.1$ (implosion).

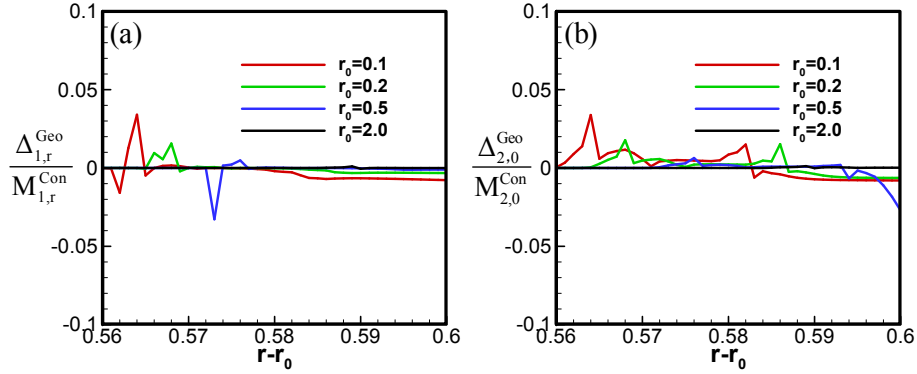


Figure 16: The profiles of (a) $\Delta_{1,r}^{Geo}/M_{1,r}^{Con}$ and (b) $\Delta_{2,0}^{Geo}/M_{2,0}^{Con}$ around the shock wave front for different cases (implosion).

density, flow velocity and temperature than the corresponding Navier-Stokes model only if the second order terms in Knudsen number in the Chapman-Enskog expansion are taken into account in the model construction. With the DBM we can study *simultaneously* both the hydrodynamic and thermodynamic behaviors. Since the inverse of the transformation matrix \mathbf{C} connecting the discrete equilibrium distribution function \mathbf{f}^{eq} and corresponding moments $\hat{\mathbf{f}}^{eq}$ has been fixed, the extension to multiple-relaxation-time DBM[56] is straightforward. As for the DBM in spherical coordinates, if consider flow behaviors near the spherical center, the “force term” (the term for geometric effects) should consider the higher order nonequilibrium effects. Specifically, $f = f^{eq}$ should be replaced by $f = f^{eq} + f^{(1)}$, even $f = f^{eq} + f^{(1)} + f^{(2)}$, etc. in the “force term”. It should also be pointed out that, fixing the transformation matrix \mathbf{C} and its inverse is only one of the possible schemes to get a solution for the discrete equilibrium distribution function \mathbf{f}^{eq} . A second way to find a solution for the discrete equilibrium distribution function \mathbf{f}^{eq} is to follow the ideas used in Refs. [52]. A difference is that the scheme introduced in this work needs the minimum number of discrete velocities.

Acknowledgements

The authors would like to thank Drs. Chuandong Lin, Yanbiao Gan and Feng Chen for helpful discussions. The work is supported by National Natural Science Foundation of China [under grant nos. 11475028,11772064 and U1530261] and Science Challenge Project (under Grant No. JCKY2016212A501 and TZ2016002).

References

References

- [1] J. Buckmaster, T. L. Jackson, A. Kumar, Combustion in High-Speed Flows, Springer Netherlands, 1994.

- [2] L. F. Wang, W. H. Ye, X. T. He, J. F. Wu, Z. F. Fan, C. Xue, H. Y. Guo, W. Y. Miao, Y. T. Yuan, J. Q. Dong, Theoretical and simulation research of hydrodynamic instabilities in inertial-confinement fusion implosions, *Science China Physics Mechanics & Astronomy* 60 (5) (2017) 055201.
- [3] A. G. Xu, G. C. Zhang, Y. J. Ying, C. Wang, Complex fields in heterogeneous materials under shock: modeling, simulation and analysis, *Science China Physics Mechanics & Astronomy* 59 (5) (2015) 650501.
- [4] Z. H. Li, H. X. Zhang, Study on gas kinetic unified algorithm for flows from rarefied transition to continuum, *Journal of Computational Physics* 193 (2) (2004) 708-738.
- [5] Z. H. Li, A. P. Peng, H. X. Zhang, J. Y. Yang, Rarefied gas flow simulations using high-order gas-kinetic unified algorithms for boltzmann model equations, *Progress in Aerospace Sciences* 74 (2015) 81-113.
- [6] A. P. Peng, Z. H. Li, J. L. Wu, X. Y. Jiang, Validation and analysis of gas-kinetic unified algorithm for solving boltzmann model equation with vibrational energy excitation, *Acta Physica Sinica* 66 (20) (2017) 204703.
- [7] Z. H. Li, A. P. Peng, F. Fang, S. X. Li, S. Y. Zhang, Gas-kinetic unified algorithm for hypersonic aerothermodynamics covering various flow regimes solving boltzmann model equation, *Acta Physica Sinica* 64 (22) (2015) 204703.
- [8] Z. Li, X. Jiang, J. Wu, A. Peng, Gas-kinetic unified algorithm for boltzmann model equation in rotational nonequilibrium and its application to the whole range flow regimes, *Chinese Journal of Theoretical & applied Mechanics* 46 (3) (2014) 336-351.
- [9] W. Lei, J. M. Reese, Y. Zhang, Solving the boltzmann equation deterministically by the fast spectral method: application to gas microflows, *Journal of Fluid Mechanics* 746 (746) (2014) 53-84.

- [10] L. Wu, J. Zhang, J. M. Reese, Y. Zhang, A fast spectral method for the boltzmann equation for monatomic gas mixtures, *Journal of Computational Physics* 298 (C) (2015) 602-621.
- [11] J. Li, C. Zhong, Y. Wang, C. Zhuo, Implementation of dual time stepping and gmres of implicit gas-kinetic scheme for unsteady flow simulations, *Physical Review E* 95 (5).
- [12] Y. Zhu, C. Zhong, K. Xu, Implicit unified gas-kinetic scheme for steady state solutions in all flow regimes, *Journal of Computational Physics* 315 (2016) 16-38.
- [13] G. H. Tang, Y. H. Zhang, X. J. Gu, D. R. Emerson, Lattice boltzmann modelling knudsen layer effect in non-equilibrium flows, *EPL* 83 (4) (2008) 226-234.
- [14] G. H. Tang, Y. H. Zhang, D. R. Emerson, Lattice boltzmann models for nonequilibrium gas flows, *Physical Review E* 77 (2) (2008) 046701.
- [15] G. H. Tang, X. J. Gu, R. W. Barber, D. R. Emerson, Y. H. Zhang, Lattice boltzmann simulation of nonequilibrium effects in oscillatory gas flow, *Physical Review E* 78 (2) (2008) 026706.
- [16] J. Meng, Y. Zhang, Kinetic diffuse boundary condition for high-order lattice boltzmann model with streaming-collision mechanism, *Journal of Computational Physics* 258.
- [17] J. Meng, Y. Zhang, Gauss-hermite quadratures and accuracy of lattice boltzmann models for nonequilibrium gas flows., *Physical Review E* 83 (3 Pt 2) (2011) 036704.
- [18] J. Meng, Y. Zhang, X. Shan, Multiscale lattice boltzmann approach to modeling gas flows, *Physical Review E* 83 (4 Pt 2) (2010) 046701.
- [19] J. Meng, N. Dongari, J. M. Reese, Y. Zhang, A kinetic switching criterion for hybrid modelling of multiscale gas flows, Vol. 362, 2012, pp. 12006-12013(8).

- [20] J. Meng, Y. Zhang, N. G. Hadjiconstantinou, G. A. Radtke, X. Shan, Lattice ellipsoidal statistical bgk model for thermal non-equilibrium flows, *Journal of Fluid Mechanics* 718 (3) (2013) 347-370.
- [21] K. Xu, J. C. Huang, A unified gas-kinetic scheme for continuum and rarefied flows, Academic Press Professional, Inc., 2010.
- [22] K. Xu, J. C. Huang, An improved unified gas-kinetic scheme and the study of shock structures, *Ima Journal of Applied Mathematics* 76 (5) (2011) 698-711.
- [23] J. C. Huang, K. Xu, P. Yu, A unified gas-kinetic scheme for continuum and rarefied flows ii: multi-dimensional cases, *Communications in Computational Physics* 12 (3) (2012) 662-690.
- [24] A. Xu, G. Zhang, Y. Zhang, Discrete Boltzmann Modeling of Compressible Flows. Chapter 2 in *Kinetic Theory* edited by G. Z. Kyzas and A. C. Mitropoulos, Croatia: InTech, 2018.
- [25] A. G. Xu, G. C. Zhang, Y. J. Ying, Progress of discrete boltzmann modeling and simulation of combustion system, *Acta Physica Sinica* 64 (18).
- [26] C. Lin, A. Xu, G. Zhang, Y. Li, S. Succi, Polar-coordinate lattice boltzmann modeling of compressible flows, *Physical Review E* 89 (11) (2014) 013307.
- [27] A. Xu, C. Lin, G. Zhang, Y. Li, Multiple-relaxation-time lattice boltzmann kinetic model for combustion, *Physical Review E* 91 (4) (2015) 043306.
- [28] Y. Gan, A. Xu, G. Zhang, S. Succi, Discrete boltzmann modeling of multiphase flows: hydrodynamic and thermodynamic non-equilibrium effects, *Soft Matter* 11 (26) (2015) 5336-5345.
- [29] H. Lai, A. Xu, G. Zhang, Y. Gan, Y. Ying, S. Succi, Thermo-hydrodynamic non-equilibrium effects on compressible rayleigh-taylor instability, *Physical Review E* 94 (2016) 023106.

- [30] C. Lin, A. Xu, G. Zhang, Y. Li, Double-distribution-function discrete boltzmann model for combustion, *Combustion & Flame* 164 (2016) 137-151.
- [31] Y. Zhang, A. Xu, G. Zhang, C. Zhu, C. Lin, Kinetic modeling of detonation and effects of negative temperature coefficient, *Combustion & Flame* 173 (2016) 483-492.
- [32] Y. Zhang, A. Xu, G. Zhang, Z. Chen, Discrete boltzmann method with maxwell-type boundary condition for slip flow, *Commun. Theor. Phys.* 69 (2018) 77-85.
- [33] Y. Gan, A. Xu, G. Zhang, H. Lai, Three-dimensional discrete boltzmann models for compressible flows in and out of equilibrium, *Proceedings of the Institution of Mechanical Engineers, Part C: Journal of Mechanical Engineering Science* 232 (3) (2017) 477-490.
- [34] C. Lin, A. Xu, G. Zhang, K. Luo, Y. Li, Discrete boltzmann modeling of rayleigh-taylor instability in bi-component compressible flows, *Physical Review E* 96 (2016) 053305.
- [35] C. Lin, K. Luo, L. Fei, S. Succi, A multi-component discrete boltzmann model for nonequilibrium reactive flows, *Scientific Reports* 7 (2017) 14580.
- [36] Y. Zhang, A. Xu, G. Zhang, Z. Chen, P. Wang, Discrete ellipsoidal statistical bgk model and burnett equations, *Front. Phys.* 13 (3) (2018) 135101.
- [37] M. L. Rocca, A. Montessori, P. Prestininzi, S. Succi, A multispeed discrete boltzmann model for transcritical 2d shallow water flows, *Journal of Computational Physics* 284 (C) (2015) 117-132.
- [38] S. Succi, *The Lattice Boltzmann Equation for Fluid Dynamics and Beyond*, Oxford University Press, New York, 2001.
- [39] S. Toppaladoddi, S. Succi, J. S. Wettlaufer, Roughness as a route to the ultimate regime of thermal convection., *Physical Review Letters* 118 (7) (2017) 074503.

- [40] X. Shan, X. Yuan, H. Chen, Kinetic theory representation of hydrodynamics: a way beyond the navier-stokes equation, *Journal of Fluid Mechanics* 550 (7) (2006) 413-441.
- [41] J. Meng, Y. Zhang, N. G. Hadjiconstantinou, G. A. Radtke, X. Shan, Lattice ellipsoidal statistical bgk model for thermal non-equilibrium flows, *Journal of Fluid Mechanics* 718 (3) (2013) 347-370.
- [42] D. Sun, M. Zhu, S. Pan, D. Raabe, Lattice boltzmann modeling of dendritic growth in a forced melt convection, *Acta Materialia* 57 (6) (2009) 1755-1767.
- [43] Y. Wang, C. Shu, H. B. Huang, C. J. Teo, Multiphase lattice boltzmann flux solver for incompressible multiphase flows with large density ratio, *Journal of Computational Physics* 280 (C) (2015) 404-423.
- [44] Z. Chai, C. Huang, B. Shi, Z. Guo, A comparative study on the lattice boltzmann models for predicting effective diffusivity of porous media, *International Journal of Heat & Mass Transfer* 98 (2016) 687-696.
- [45] H. Liu, L. Wu, Y. Ba, G. Xi, A lattice boltzmann method for axisymmetric thermocapillary flows, *International Journal of Heat & Mass Transfer* 104 (2017) 337-350.
- [46] L. Chen, L. Zhang, Q. Kang, H. S. Viswanathan, J. Yao, W. Tao, Nanoscale simulation of shale transport properties using the lattice boltzmann method: permeability and diffusivity, *Scientific Reports* 5 (2015) 8089.
- [47] C. Zhuo, C. Zhong, J. Cao, Filter-matrix lattice boltzmann model for incompressible thermal flows., *Physical Review E* 85 (4 Pt 2) (2012) 046703.
- [48] J. Meng, Y. Zhang, Diffuse reflection boundary condition for high-order lattice boltzmann models with streaming - collision mechanism, *Journal of Computational Physics* 258 (C) (2014) 601-612.

- [49] L. Wang, G. Zhou, X. Wang, Q. Xiong, Direct numerical simulation of particle-fluid systems by combining time-driven hard-sphere model and lattice boltzmann method, *Particuology* 8 (4) (2010) 379-382.
- [50] A. Doostmohammadi, T. N. Shendruk, K. Thijssen, J. M. Yeomans, Onset of meso-scale turbulence in active nematics, *Nature Communications* 8 (2017) 15326.
- [51] A. G. Xu, G. C. Zhang, Y. B. Gan, F. Chen, X. J. Yu, Lattice boltzmann modeling and simulation of compressible flows, *Frontiers of Physics* 7 (5) (2012) 582-600.
- [52] M. Watari, M. Tsutahara, Possibility of constructing a multispeed bhatnagar-gross-krook thermal model of the lattice boltzmann method, *Physical Review E* 70 (2) (2004) 016703.
- [53] H. Liu, W. Kang, Q. Zhang, Y. Zhang, H. Duan, X. T. He, Molecular dynamics simulations of microscopic structure of ultra strong shock waves in dense helium, *Frontiers of Physics* 11 (6) (2016) 1-11.
- [54] H. Liu, Y. Zhang, W. Kang, P. Zhang, H. Duan, X. T. He, Molecular dynamics simulation of strong shock waves propagating in dense deuterium, taking into consideration effects of excited electrons, *Physical Review E* 95 (2-1) (2017) 023201.
- [55] H. Liu, W. Kang, H. Duan, P. Zhang, X. He, Recent progresses on numerical investigations of microscopic structure of strong shock waves in fluid, *Scientia Sinica Physica Mechanica and Astronomica* 47 (7) (2017) 070003.
- [56] F. Chen, A. G. Xu, G. C. Zhang, Y. L. Wang, Two-dimensional multiplerelaxation-time lattice boltzmann model for compressible and incompressible flows, *Frontiers of Physics* (2) (2014) 246-254.